CHARACTERISTIC MICROSTRUCTURE FEATURES AND THEIR EFFECTS ON RESTRAINED AUTOGENOUS SHRINKAGE BEHAVIOR IN HIGH STRENGTH CONCRETES AT AN EARLY AGE

(Translation from Proceedings of JSCE, No.704/V-55, May 2001)



Shin-ichi IGARASHI Mitsunori KAWAMURA Takashi MORISHITA

Fluorescence microscopy examinations are used to identify the damage induced as a result of restraining autogenous shrinkage. The characteristics of fluorescent areas and correlation with the autogenous shrinkage behavior of high strength concretes are discussed. The results show that silica fume concrete exhibits greater creep potential when loaded at a very early age. Sealed concrete microstructures are porous, especially at aggregate particle interfaces. Further, sealed silica fume concretes contain many Hadley grains. These microstructure features are not observed in water-ponded concretes. The fluorescing areas may be defects caused by self-desiccation and autogenous shrinkage. They have little effect on strength development. However, the presence of narrow openings around remnant cement particles may increase creep deformation to relieve internal stresses.

Key Words: *autogenous shrinkage, silica fume, tensile creep, restraining stress, Hadley grain*

Shin-ichi Igarashi is an associate professor in the Department of Civil Engineering at Kanazawa University, Kanazawa, Japan. His research interest is the microstructure of cementitious materials. He is a member of the JSCE, JCI, JSMS, ACI, and RILEM.

Mitsunori Kawamura is a professor in the Department of Civil Engineering at Kanazawa University, Kanazawa, Japan. His research interests include concrete durability. He is a member of the JSCE, JCI, JSMS, and ACI.

Takashi Morishita is a research engineer with the Nagoya Municipal Government, Japan. He obtained his Master of Engineering degree from Kanazawa University in 2001. He is a member of the JSCE.

1. Introduction

Cement hydration is the process by which a solid structure is formed in spaces previously occupied by water. In a case where no external water is supplied to a cement paste with a low water/cement ratio, the relative humidity of the system decreases as hydration proceeds. Such early drying results in volume changes of the premature concrete. Plastic shrinkage is a well-known phenomenon that results from early-age volume changes caused by drying. Cracking that would otherwise result from this plastic shrinkage is avoided by applying suitable curing methods to block loss of water from the surface by evaporation. However, when the water/cement ratio is extremely low, self-desiccation can occur as water is consumed by hydration, even if water curing is applied to the concrete. The menisci that develop as a result of self-desiccation cause capillary stresses, which then result in autogenous shrinkage of early-age concrete [1].

Generally, autogenous shrinkage and self-desiccation have little effect on the performance of conventional concretes with high water/cement ratios. Consequently, little attention has been paid to their effects on concrete properties. However, autogenous shrinkage can be particularly severe in high strength concretes with low water/cement ratios. The restraint of autogenous shrinkage can induce cracking, since the early-age strength of concrete is not sufficient to resist the stresses caused by external and internal restraints [1]. Such early age cracking may have an adverse effect on the long-term durability and mechanical properties of high strength concrete [2].

In Japan, research into autogenous shrinkage includes extensive studies by Tazawa and Miyazawa [3] over the past ten years. Also, the Japan Concrete Institute established a technical committee on autogenous shrinkage in 1994. The mechanisms of autogenous shrinkage, test methods, and design considerations for high strength concretes with low water/cement ratios have been extensively investigated in detail. The results of these activities were published as state-of-the-art reports in 1998 and 2002 [4,5]. At present, more advanced and comprehensive investigations are in progress with the aim of establishing a rational methodology for the use and design of high strength concretes in terms of early cracking risk and restraining stress estimation [6].

Cracking and internal stress generation are significantly influenced by the growth of the internal solid structure at an early age. However, few studies have attempted to relate features of the microstructure at an early age to restrained shrinkage behavior in high strength concretes [7,8,9]. In this study, fluorescence microscopy examinations are conducted to identify the damage induced by self-desiccation and the restraint of autogenous shrinkage. The characteristics of fluorescence areas detected in high strength concrete at an early age are discussed in relation to viscoelastic behavior as evaluated through closed-loop uniaxial restrained shrinkage tests. The effects of water ponding [10] and the incorporation of silica fume on shrinkage behavior are also discussed, with emphasis on changes in microstructure as revealed by fluorescence microscopy, quantitative analysis of backscattered electron images, and microhardness measurements.

2. Experimental

2.1 Concrete materials and mix proportions

The cement used was ordinary Portland cement. A silica fume with specific surface area of 20 m^2/g was used. The replacement ratio of silica fume was 10%. River gravel with a maximum size of 10 mm was used as the coarse

Table 1 Mix proportion of concretes

	Unit Content (kg/m^3)						Superplasticizer (%wt.B)
	W/B	Water	Cement	Silica Fume	Sand	Gravel	
PC	0.25	145	581	0	559	1086	1.7
SF	0.25	142	510	57	559	1086	2.6
PC	0.33	168	509	0	559	1086	1.3
SF	0.33	165	449	50	559	1086	2.0

aggregate. The fine aggregate was a river sand. A polycarboxylic acid superplasticizer was used. Two water/binder ratios were used: 0.25 and 0.33. The mix proportions of the concretes are given in Table 1. In experiments using cement paste specimens, the dosage of superplasticizer was adjusted to attain adequate workability without excess bleeding.

2.2 Restrained and free shrinkage tests

The restrained and free shrinkage tests were carried out on sealed specimens at 18°C. Concrete was cast directly into the molds of the restrained and free shrinkage test apparatus (Fig. 1) [11]. In order to reduce friction between the cast concrete and the mould, the mold was lined with thin plastic sheet. This system, developed by Kovler [11], can be used to determine free shrinkage, restraining stresses, and viscoelastic response using the procedures outlined in Kovler's paper (Fig.2). The specimens were sealed immediately after casting. As for the water-ponded specimens, the top surfaces were fully covered with thick sponge saturated with water. The sponge was wetted every day to ensure that the concrete remained in saturated condition.

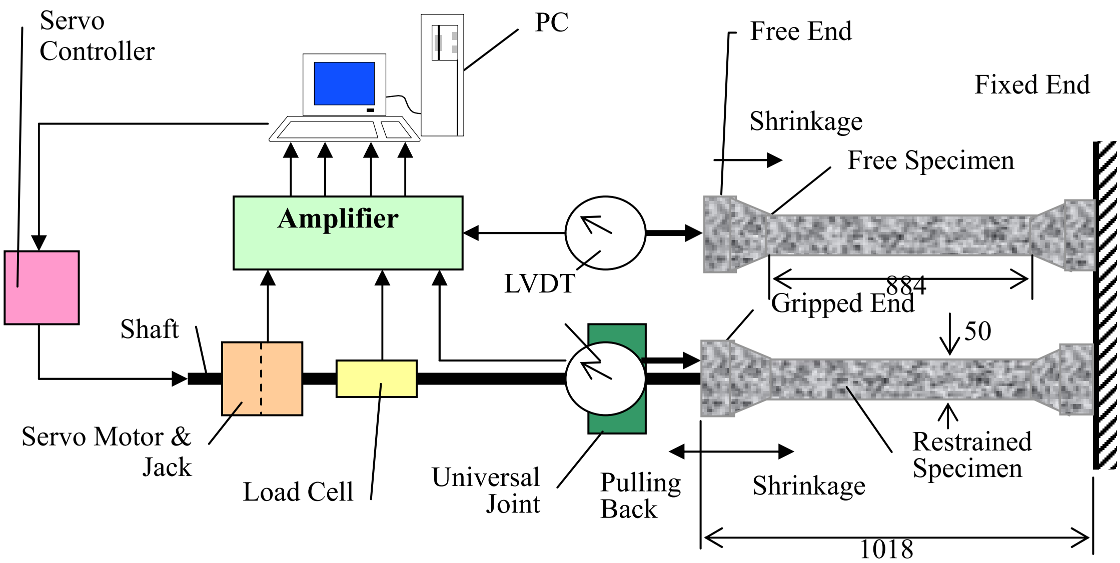

Fig.1 Restrained shrinkage test apparatus

The two types of test are carried out on identical specimens with identical measuring devices. In the restrained shrinkage tests, as shrinkage causes the strain to exceed 10×10^{-6}, a servo motor automatically pulls the specimen back to its initial position. This movement of the grip corresponds to the increment in elastic strain ($\Delta\varepsilon_{el}$). The elastic strain cancels the shrinkage strain ($\Delta\varepsilon_{sh}$) and the creep strain ($\Delta\varepsilon_{cr}$). The shrinkage strain is obtained from the free shrinkage strain of the free specimen. The loading system is designed such that the total deformation of a restrained specimen is always zero at each increment of elastic strain, as follows:

$$\varepsilon_{total} = \varepsilon_{sh} + \varepsilon_{el} + \varepsilon_{cr} = 0 \tag{1}$$

where,

ε_{sh} : cumulative shrinkage strain

ε_{el} : cumulative elastic strain

ε_{cr} : cumulative creep strain

The sum of elastic strains up to a particular time is equal to the sum of the shrinkage and creep strains in absolute value (Eq. (2)).

$$\varepsilon_{el} = -(\varepsilon_{sh} + \varepsilon_{cr}) \tag{2}$$

Therefore, the cumulative creep strain up to a given time τ_k is given by Eq. (3).

$$\varepsilon_{cr}(\tau_k) = -\frac{1}{2}\sum_{i=0}^{k}\{\varepsilon(\tau_i) - \varepsilon(\tau_{i-1})\} - \varepsilon_{sh}(\tau_k) \tag{3}$$

where,
$\varepsilon_{cr}(\tau_k)$: cumulative creep strain at time τ_k
$\varepsilon_{sh}(\tau_k)$: shrinkage strain at time τ_k
$\varepsilon(\tau_i)$: measured strain at time τ_i

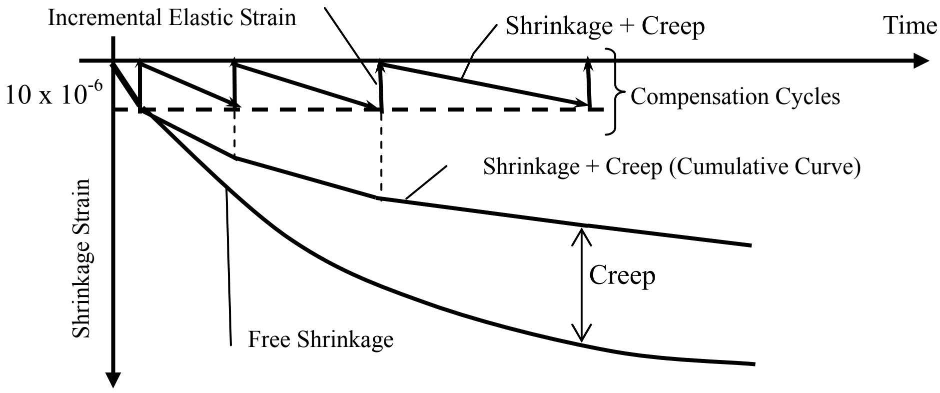

Fig. 2 Creep strain calculated using data from restrained autogenous shrinkage tests

The specific creep is calculated by dividing the cumulative creep strain by the total restraining stress at a given time [12,13]. The length changes of both specimens and the restraining load generated by the restrained shrinkage specimen were continuously recorded. Restraint was applied to the specimen after allowing it to shrink for the first 12 hours. Testing continued for seven days after casting.

2.3 Strength tests

Cylinder specimens measuring 50 mm in diameter by 100 mm in height were produced. They were cured under the same conditions as the specimens for the shrinkage tests. Splitting tensile strength and compressive strength tests were carried out at the ages of 1, 3, and 7 days. Specimens used in the shrinkage tests were also tested for splitting tensile strength.

2.4 Fluorescence microscopy

Slices measuring about 10 mm in thickness were cut from the mid-point of specimens previously used for the shrinkage tests. The slices were immersed in ethanol, and then impregnated with epoxy resin containing a fluorescence dye. After hardening the resin at room temperature, the slices were polished with silicon carbide paper in preparation for fluorescence microscopy examinations.

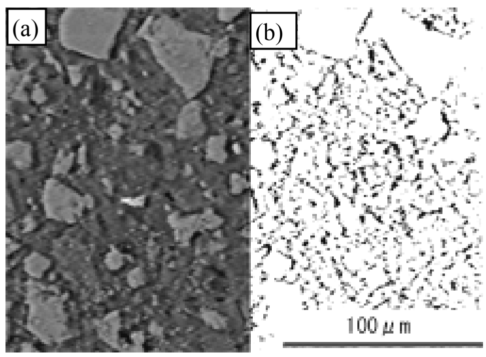

Fig.3 An example of BSE image (a) and binary segmentation of image for pores (b) (Silica fume-free with a water/binder ratio of 0.25, Age=24hours)

2.5 Microhardness measurements

Cement paste specimens containing only coarse aggregate were produced. The volume fraction of coarse aggregate was 10%. These specimens were cured under the same conditions as those used in the shrinkage tests. At the age of seven days, slices were cut from the specimens. The surfaces of the slices were polished. A microhardness tester with a Vickers indenter (load = 0.1 N) was used to measure microhardness in the cement paste phase around aggregate grains.

2.6 BSE image analysis

Cylinders measuring 100 mm in length and 50 mm in diameter were produced. They were cured under the same conditions as the specimens for the shrinkage tests. At the ages of 12 and 24 hours, slices measuring about 10 mm in thickness were cut for use in BSE image analysis. They were dried by ethanol replacement and vacuum drying, and then impregnated with a low-viscosity epoxy resin. After the resin had hardened at room temperature, the slices were finely polished with silicon carbide paper. The polished surfaces were meticulously finished with diamond slurry for a short time.

Samples were examined using a scanning electron microscope (SEM) equipped with a quadruple backscatter detector. BSE images were acquired at a magnification of 500 x. In order to avoid the influence of interfacial transition zones around fine aggregate particles, regions of interest for acquiring images were chosen sufficiently distant from aggregate particles. Each BSE image consists of 1,148 x 1,000 pixels, with one pixel representing about 0.22 x 0.22μm. The dynamic thresholding method was used to make a binary segmentation based on the gray level histogram. Pixels for unhydrated cement particles and pores were tallied so as to obtain area fractions of the phases [14]. Based on stereology principles, area fractions in 2D cross sections were assumed to be equal to 3D volume fractions. It was also assumed that volume fractions of hydration products (i.e. CSH and calcium hydroxide crystals) could be obtained by subtracting the volume of unhydrated cement particles and capillary pores from the total volume of a sample. A typical BSE micrograph of a young cement paste and its binary segmentation are shown in Fig. 3.

3. Results

3.1 Autogenous shrinkage behavior of sealed concrete

(1) Autogenous shrinkage strain and evolution of restraining stress

Figure 4 shows the free autogenous shrinkage for cement pastes with and without silica fume. Regardless of the presence of silica fume, a dramatic increase in autogenous shrinkage strain was observed within the initial 10-15 hours of casting. However, subsequent changes were less notable. The paste containing silica fume exhibited greater shrinkage than the one without. Tensile failure occurred in the silica fume specimen at the age of 5.5 days; the length change of this specimen had approached the ultimate shrinkage strain allowed for the test apparatus in this study (about 1900 x 10^{-6}).

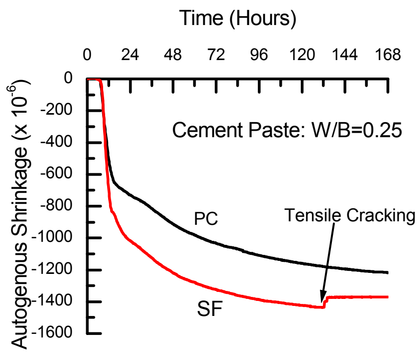

Fig. 4 Free autogenous shrinkage strain of cement paste specimens with and without silica fume

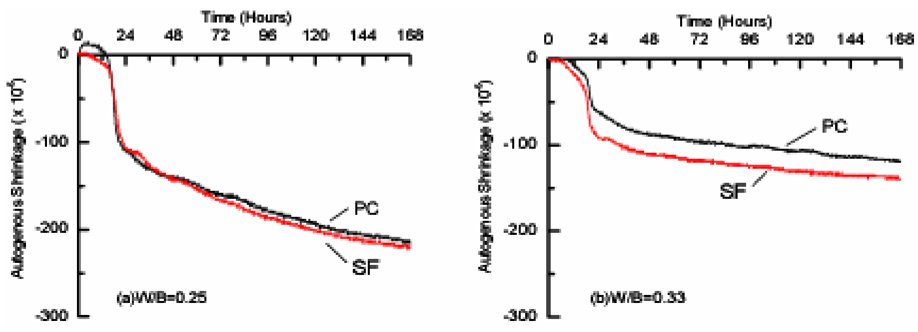

Fig.5 Free autogenous shrinkage strain of concretes

Figure 5 shows the free autogenous shrinkage for concretes with water/binder ratios of 0.25 and 0.33. Autogenous shrinkage strain increased rapidly during the first 24 hours. However, the rate of shrinkage fell thereafter. Little difference was seen in the free autogenous shrinkage strain between concretes with and without silica fume. It has previously been pointed out that the addition of silica fume increases the autogenous shrinkage of cement paste [1], and this is backed up by Fig. 4. However, it seems that silica fume concrete does not always exhibit greater shrinkage strain than silica fume-free concrete, since aggregate particles have a diluting effect and restrain shrinkage of the surrounding cement paste matrix.

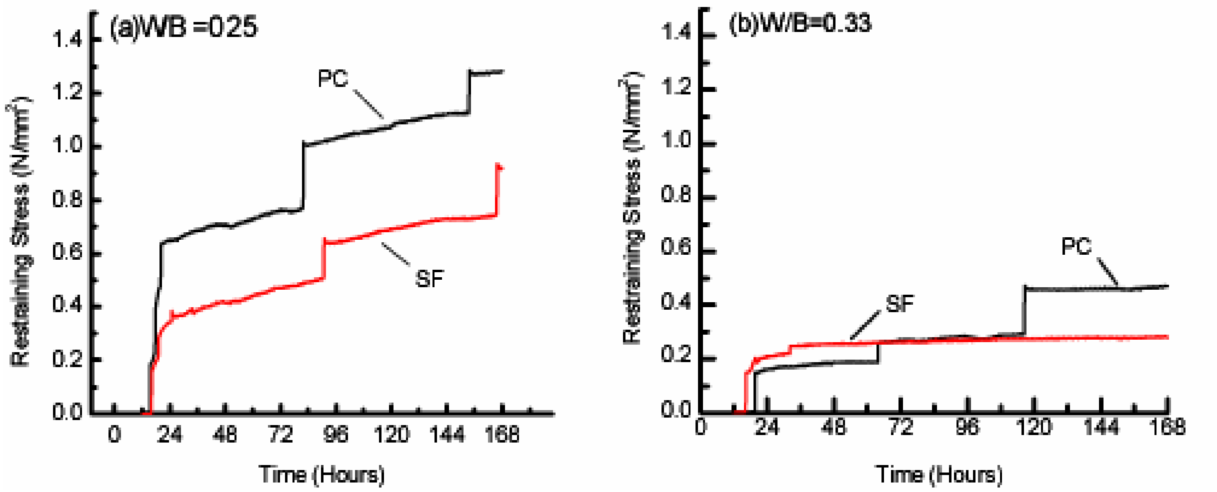

Fig.6 Development of restraining stress

Figure 6 shows the development of restraining stress with time. Step-wise increases in restraining stress are observed here since compensation for strain by the movable grip took place in fixed increments. The restraining stress generated in the silica fume-free concrete with a water/binder ratio of 0.25 was greater than that in the silica fume concrete with the same water/binder ratio, whereas the free shrinkage strain was almost the same in the two cases. The stresses induced in concretes with a water/binder ratio of 0.33 were considerably smaller than those in concretes with a water/binder ratio of 0.25. The restraining stress in the silica fume concrete with a water/binder ratio of 0.33 was also smaller than that of silica fume-free concrete at the age of 120 hours.

Figures 5 and 6 make clear that restraining stress cannot be determined from only the absolute values of free autogenous shrinkage. The viscoelastic properties of early-age concrete need to be taken into account when resolving the evolution of stress under restraint [4,5].

(2) Total creep strain and specific creep

Figure 7 shows increase in creep strain with time in the restrained specimens. The presence of silica fume in the concrete had little influence on the amount of strain. Comparing Fig. 7 with Fig. 5, it can be seen that

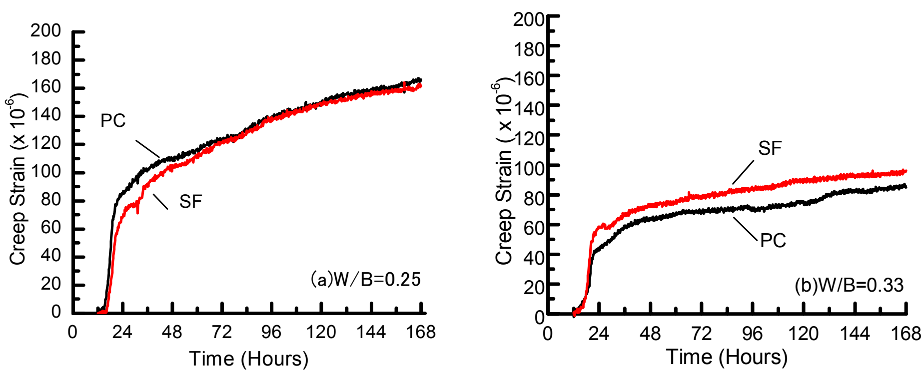

Fig.7 Creep strain in restrained shrinkage specimens

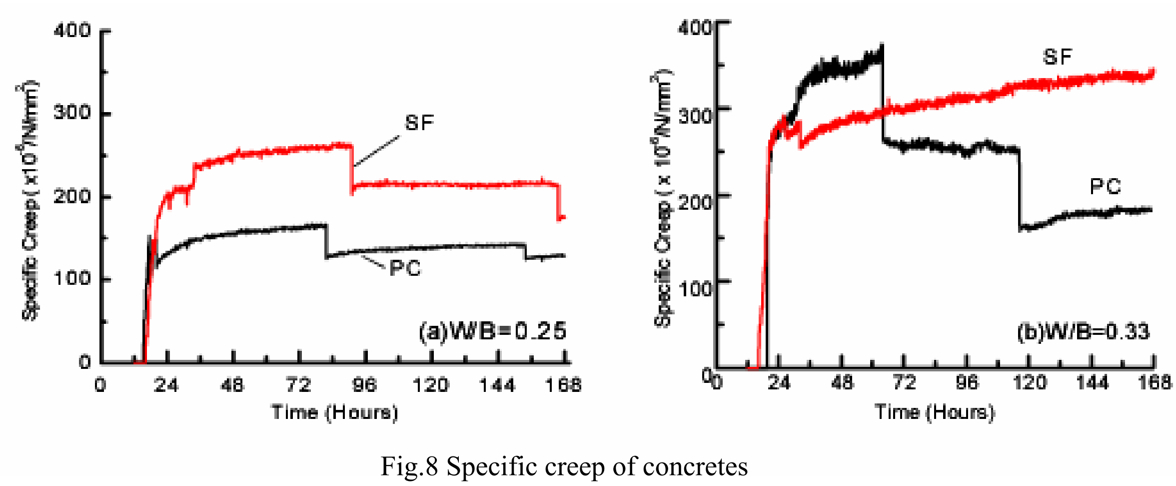

Fig.8 Specific creep of concretes

most of the free autogenous shrinkage was compensated by creep. This large creep strain leads to relaxation of stress in the restrained concrete.

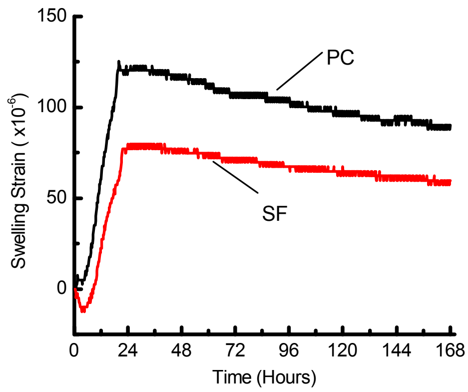

Fig.9 Swelling strain in water-ponded concretes

In contrast with the total creep strain shown in Fig. 7, significant differences are seen in specific creep, a value obtained by normalizing the total creep strain by the total restraining stress (Fig. 8). Silica fume concrete exhibited greater specific creep than concretes without silica fume at a water/binder ratio of 0.25, even though there was little difference in total autogenous shrinkage and creep strain between the two. The change in specific creep with time was relatively small after the first 24 hours. The specific creep of concretes with a water/binder ratio of 0.25 fell slightly with time. The characteristics of this change were different for concretes with water/binder ratios of 0.33 and 0.25. The specific creep of concrete with no silica fume and a water/binder ratio of 0.33 decreased with time, since the restraining stress increased with age. The specific creep of silica fume concrete with a water/binder ratio of 0.33 was greater than that of silica fume-free concrete at an age of 168 hours.

It is well known that mature silica fume concrete exhibits smaller creep deformation under compressive loading than concrete without silica fume. This lower creep potential results from the higher strength and denser microstructure at the time when loading takes place. However, in this study, the specific tensile creep of silica fume concrete was greater than that of concrete without silica fume. Greater creep deformation in silica fume concrete under tensile

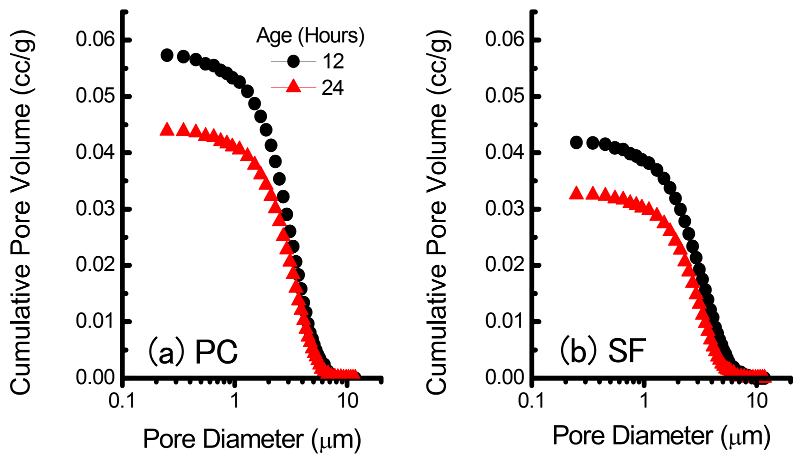

Fig.10 Coarse capillary pore size distributions at early age (W/B=0.25)

loading at an early age has also been reported by Bissonnette and Pigeon [15]. Similarly, Pane and Hansen [16] have also shown that the incorporation of silica fume increases tensile creep deformation, in contrast with the influence of fly ash and blast furnace slag. They attributed the greater potential for tensile creep deformation of silica fume concrete to the high pozzolanic reactivity of silica fume. It seems that greater creep is a characteristic of silica fume concrete that is exhibited under tensile loading at an early age.

(3) Reduction of autogenous shrinkage by water curing

Autogenous shrinkage is usually explained in terms of self-desiccation, which gives rise to capillary tension. In order to avoid the risk of early-age cracking due to self-desiccation, the recommendation has been to carry out water curing by ponding at an early age or to use saturated lightweight aggregate [10,17,18]. Figure 9 shows the free autogenous shrinkage of concretes kept sufficiently wet immediately following casting. In contrast with sealed concrete specimens, these concretes exhibited rapid swelling for the first 24 hours. The swelling strain of concrete without silica fume was greater than that of silica fume concrete. Thereafter, however, the concretes began shrinking, and the differences in swelling strain between the two types decreased with time. Figure 9 confirms that water ponding is an effective method of avoiding autogenous shrinkage and the generation of restraining tensile stresses.

3.2 Early-age pore structure

Figure 10 shows the coarse capillary pore size distribution in high strength concretes with and without silica fume, indicating that silica fume concretes have fewer coarse pores than ordinary concretes even at the very early ages of 12 and 24 hours. Generally, total porosity does not change with the addition of silica fume, as long as the concrete is produced with the same water/binder ratio [19]. Differences in the total porosity and pore size distribution curves for concretes with and without silica fume (Fig. 10) indicate that concrete containing silica fume has greater numbers of pores finer than the image resolution (or smaller than about 0.2 μm in diameter) than ordinary concrete. Park, Noguchi, and Tomosawa [20] have measured the porosity of cement pastes at an early age by the mercury intrusion

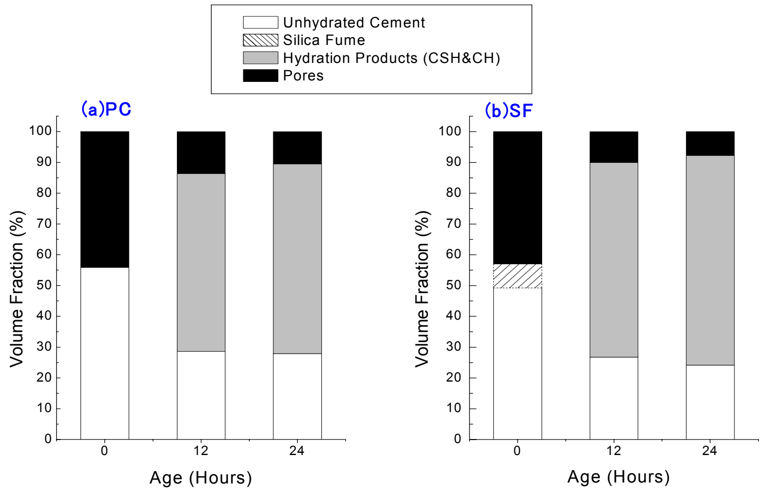

Fig.11 Volumetric fractions of various concrete constituents at early age (W/B=0.25)

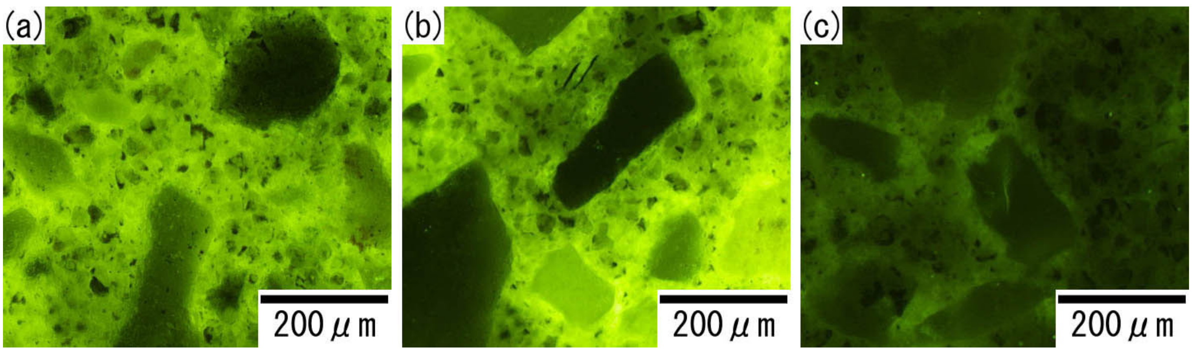

Fig.12 Fluorescence micrographs of concretes without silica fume (W/B=0.25)
(a) Sealed (free) (b) Sealed (restrained) (c) Water-ponded

porosimetry (MIP) method. According to their results, the total porosity of ordinary Portland cement pastes with a water/cement ratio of 0.25 is about 0.12 and 0.08 cc/g at 12 and 24 hours of age, respectively. A direct comparison in pore size distributions between the data obtained by both methods cannot be treated as significant. However, we can compare the total porosity obtained by the two methods. The fine porosity (pores less than 0.2 μm in diameter) of silica fume-containing concrete is 40% greater than that of concrete without silica fume. This clearly demonstrates that concretes containing silica fume have more finer pores. In other words, more refined pore structures have already been formed in such concretes within 24 hours of casting.

Figure 11 shows the volumetric fractions of various concrete constituents in the two types of concrete. The volume fractions of hydration products in silica fume concretes are found to be greater than those in ordinary concretes. However, these fractions of hydration products at 12 and 24 hours include unreacted silica fume. However, it is known that the pozzolanic reaction of silica fume begins at a very early stage [21], so if it is assumed that half of the silica fume reacts within 24 hours of mixing [21], the net volume fraction of hydration products in silica fume-containing concretes is greater than that of ordinary concretes (Fig. 11). Furthermore, remembering that the mean size of silica fume particles is of the same order as that of hydration products, it can be assumed that the remaining silica fume particles are themselves involved in forming the finer porous microstructure. Increased amounts of hydration products with less $Ca(OH)_2$ crystals and a more refined pore structure (Figs. 10 and 11) may be consistent with the increase in autogenous shrinkage in systems containing silica fume (Fig. 4)[9].

3.3 Fluorescence microscopy and microhardness measurements

Figure 12 shows fluorescence micrographs of the polished surface of concrete specimens without silica fume. Regardless of the restraint conditions, the whole of the mortar matrix of concrete cured under sealed conditions is found to fluoresce quite brightly under the microscope. Furthermore, the area around aggregate grains is brighter than the bulk cement paste matrix. Brighter fluorescence equates to greater porosity. This demonstrates that the cement paste matrix of concretes cured without an external supply of water is extremely porous, particularly in the vicinity of aggregate grains. On the contrary, the matrix in water-ponded concrete specimens is much darker. Water ponding at a very early age results in the formation of a dense microstructure.

Fluorescence micrographs for silica fume concretes are shown in Fig. 13. These concretes have a very dense microstructure compared to those without silica fume. However, as seen in Fig. 13(b), regions brighter than the bulk matrix are visible around aggregate grains where the concrete was sealed (as marked by arrows #1). It should be noted that there are many remnant cores of cement particles of which peripheries were profiled by thin fluorescent areas in the sealed silica fume concretes (eg. shown by the arrows #2). These are distributed throughout the cement matrix. However, bright peripheries around cement particles were not observed in concretes supplied with adequate water during initial curing (Fig. 13(c)). Given that no bright fluorescent regions around aggregate grains and no bright peripheral regions around remaining cement particles are seen in the case of ponded concretes, these porous areas can be attributed to self-desiccation in

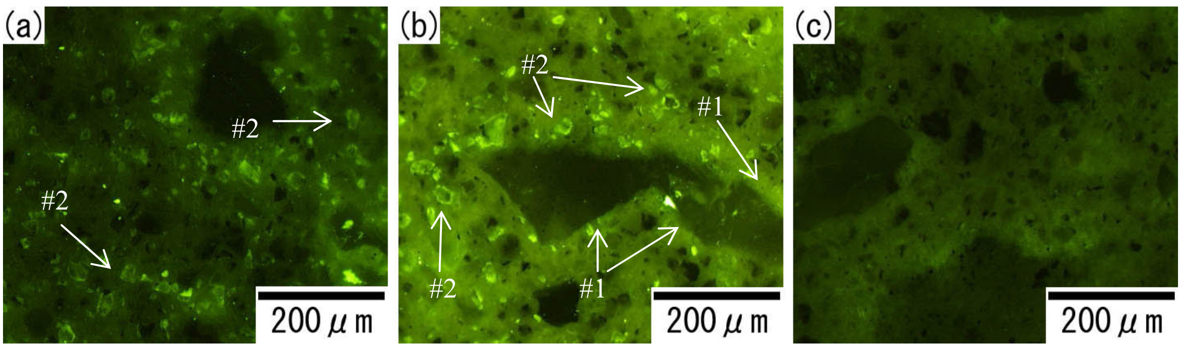

Fig.13 Fluorescence micrographs of silica fume concretes (W/B=0.25)
(a) Sealed (restrained) (b) Sealed (restrained)[long exposure time] (c) Water-ponded

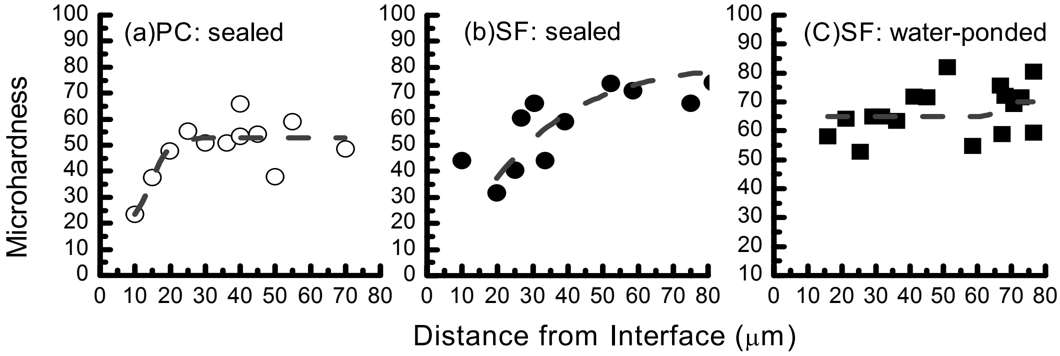

Fig.14 Microhardness distribution in vicinity of aggregate

silica fume concretes with an extremely low water/binder ratio.

Values of measured microhardness around aggregate grains are plotted in Fig. 14. In the case of sealed specimens, microhardness is lower around aggregate grains than in the bulk cement paste matrix. Thus the microhardness measurements indicate that weak microstructures are formed around aggregate grains in sealed specimens with an extremely low water/binder ratio. However, such weak regions around aggregate grains are not present in the case of ponded specimens.

4. Discussion

4.1 Damage induced by self-desiccation and restraining stresses

Internal stresses develop in response to restraint of autogenous shrinkage, as demonstrated in Fig. 6. Generally, it is considered that microcracks occur if such stresses exceed the tensile strength [22]. However, as shown in Figs. 13 and 14, no cracks are visible under the fluorescence microscope. Figure 15 shows the variations in the ratio of restraining stress to tensile strength in the restrained concrete specimens. The ratios for concretes with water/binder ratios of 0.25 and 0.33 are always less than 0.20, regardless of whether the concrete contains silica fume or not. They are found to be far less than the critical values above which microcracks form. Therefore, no serious damage was caused to the concrete by the restraining stress in this study. The splitting tensile strengths after restrained shrinkage tests are given in Table 2. A minor decrease in strength is seen in concretes subjected to the restraining stress.

On the other hands, as shown in Fig. 12, sealed specimens exhibited a porous microstructure as compared with the water-ponded ones. This porous microstructure results from a lack of water at an early age. The inadequate supply of water must have interrupted further hydration of the cement.

Generally, the interfacial transition zone around an aggregate particle is considered a weak region. However, no weakness was detected here in water-ponded concrete. Furthermore, since the concretes with an extremely low water/binder ratio contain silica fume, the bright areas seen around aggregate particles cannot be attributed to the formation of an interfacial transition zone. Therefore, these bright regions suggest the presence of invisible microcracks. Such damage may be induced by the restraint of rigid aggregate grains against autogenous shrinkage of the surrounding matrix [23]. Indeed, this is consistent with the fact that the bright areas were not present in concretes where shrinkage was reduced by water curing.

4.2 Role of aggregate grains in autogenous shrinkage of silica fume concrete

As shown in Fig. 4, pastes containing silica fume exhibited greater autogenous shrinkage than pastes made with ordinary Portland cement. A more refined pore structure and more CSH gel developed in silica fume pastes, accompanying the greater shrinkage strain (Fig. 10). However, as regards the concrete specimens

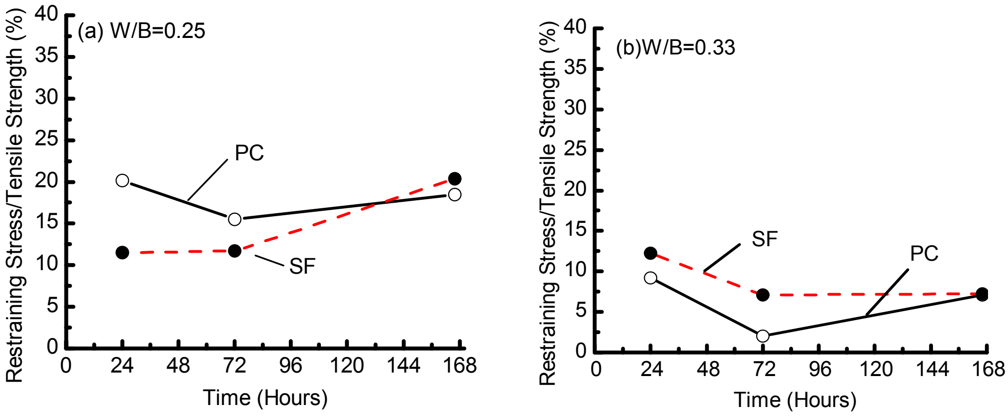

Fig. 15 Ratios of restraining stress/splitting tensile strength

corresponding to these pastes, the silica fume concrete did not always exhibit greater shrinkage than ordinary concrete.

Coarse aggregate particles have two effects on the shrinkage behavior of concrete. One is dilution of shrinkage, as mentioned previously. The other is restraint of mortar matrix shrinkage. Tazawa and Miyazawa [24] have shown that concrete shrinkage can be calculated from the volume fractions of aggregate and paste matrix. However, in this study, the shrinkage of the silica fume concrete cannot be explained by the dilution effect. On the other hand, as given in Fig. 15, the ratio of restraining stress to tensile strength is at most 20%. Iriya, Hattori, and Umehara [25] have pointed out that aggregate particles are sufficiently effective for restraining the deformation of the surrounding cement paste matrix at a stress / strength ratio of 0.2. Actually, as shown in Fig. 14, the values of microhardness around aggregate particles were higher in silica fume concrete than in ordinary concrete. This suggests that the aggregate particles in silica fume concrete have a greater restraining effect, so that the overall autogenous shrinkage of silica fume concrete was almost the same as that of ordinary concrete.

Table 2 Splitting tensile strength of concretes after the shrinkage tests (N/mm^2)

Water/Binder	0.25		0.33	
	PC	SF	PC	SF
Free Specimens	4.99	5.03	3.84	3.88
Restrained Specimens	4.24	4.45	3.64	3.78

4.3 Effects of microstructure on tensile creep in concrete loaded at an early age

From Fig. 14, it can be seen that silica fume concretes at an early age had many bright fluorescent areas along the peripheries of remaining cement particles over the entire cement paste matrix. SEM examinations at a higher magnification revealed that there were small gaps between the core cement particles and the surrounding cement paste matrix. These were very similar to those caused by hollow shell hydration of cement particles [26]. Kjelsen and Atlassi [27] have pointed out that many Hadley grains are present in a silica fume–containing system with a low water/binder ratio. Greater chemical shrinkage due to the pozzolanic reaction of silica fume and the accelerated hydration of cement in a low-water environment may be related to the insufficient filling around remaining cement particles. Unhydrated cement particles function as inclusions in the cement paste matrix on the microscopic scale. However, cement particles separated from the matrix by gaps must be less effective at confining the deformation of the cement paste matrix [28]. Furthermore, silica fume reacts with $Ca(OH)_2$ at an early stage of cement hydration, so relatively large amounts of colloidal CSH gel are produced at this time [21]. Namely, the incorporation of silica fume at extremely low water/binder ratios will lead to the formation of large amounts of CSH gel as a source of creep deformation. However, the function of unhydrated cement particles as deformation arresters is lower, as stated above. The greater tensile creep potential for relieving restraining stress in silica fume concrete at an early age reflects the microstructure characteristics of concretes with extremely low water/binder ratios.

5. Conclusions

(1) Sealed concrete is more porous than concrete cured in water.

(2) Water ponding at an early age effectively blocks autogenous shrinkage of high strength concrete. A dense microstructure is formed in water-ponded concrete.

(3) Weak regions develop around aggregate grains in sealed concrete. The restraint provided by rigid aggregate grains against autogenous shrinkage causes invisible microcracks in the vicinity of aggregate grains.

(4) Silica fume concrete contains many remaining core cement particles surrounded by fine gaps at an early age. These particles disappear if sufficient water is supplied to the system.

(5) The reduced effectiveness of cement particles surrounded by gaps may account for the greater creep potential of silica fume concrete at an early age.

References

[1] Tazawa, E., and Miyazawa, S.: Influence of binder and mix proportion on autogenous shrinkage of cementitious materials, Journal of Materials, Concrete Structures and Pavement, JSCE, No.502/V-25, pp.43-52, 1994 (in Japanese)
[2] de Larrard, F., and Bostvironnois, J.-L.: On the long-term strength losses of silica-fume high strength concretes, Magazine of Concrete Research, Vol.43, No.155, pp.109-119, 1991
[3] Tazawa, E., Miyazawa, S., and Kasai, T.: Shrinkage due to chemical reaction of cement and intrinsic voids in hardened cement paste, Review of the 40th general meeting, The Cement Association of Japan, pp.74-77, 1986
[4] JCI Committee Report: Technical Committee on Autogenous Shrinkage of Concrete, Japan Concrete Institute, 1996 (in Japanese)
[5] JCI Committee Report: State-of-the-Art Report on Autogenous Shrinkage of Concrete, Japan Concrete Institute, 2002 (in Japanese)
[6] Yang, Y., Sato, R., Imamoto, K., and Xu, M.: Estimation of stresses of high strength concrete due to autogenous shrinkage, Proc. of the Japan Concrete Institute, Vol.19, No.1, pp.757-762, 1997
[7] Takahashi, T., Nakata, H., Yoshida, K., and Goto, S.: Autogenous shrinkage of cement paste during hydration, Proc. of the 10th Intl. Congress on the Chemistry of Cement, Gothenburg, Sweden, Vol.2, 2ii070, 1997
[8] Jensen, O.M., and Hansen, P.F.: Autogenous deformation and change of the relative humidity in silica fume-modified cement paste, ACI Materials Journal, Vol.93, No.6, pp.539-543, 1996
[9] Baroghel-Bouny, V., and Kheirbek, A.: Effect of mix-parameters on autogenous deformations of cement pastes – microstructural interpretations, Shrinkage of Concrete, Shrinkage 2000, Proc. Intl. RILEM Workshop, RILEM Proc. Vol.17, pp.115-141, 2000
[10] Aitcin, P.-C.: The art and science of high performance concrete, Proc. of Mario Collepardi Symp. on Advances in Concrete Science and Technology (ed. Mehta, P.K.), pp.107-121,1997
[11] Kovler, K: Testing system for determining the mechanical behavior of early age concrete under restrained and free Uniaxial shrinkage, Materials and Structures, Vol.27, No.170, pp.324-330, 1994
[12] Kovler, K., Igarashi, S., and Bentur, A.: Tensile creep behavior of high strength concretes at early ages, Materials and Structures, Vol.312, No.219, pp.383-387, 1999
[13] Pigeon, M., Toma, G., Delagrave, A., et al: Equipment for the analysis of the behavior of concrete under restrained shrinkage at early ages, Magazine of Concrete Research, Vol.52, No.4, pp.297-302, 2000
[14] Scrivener, K.L., Patel, H.H., Pratt, P.L., and Parrott, L.J.: Analysis of phases in cement paste using backscattered electron images, methanol adsorption, and thermogravimetric analysis, Materials Research Society Proceedings, Vol.85, pp.67-76, 1987
[15] Bissonnette, B., and Pigeon, M.: Tensile creep at early ages of ordinary, silica fume, and fiber reinforced concretes, Cement and Concrete Research, Vol.25, No.5, pp.1075-1085, 1995
[16] Pane, I., and Hansen, W.: Early age creep and stress relaxation of concrete containing blended cement, Proc. of RILEM Intl. Conf. on Early Age Cracking in Cement Systems (eds. Kovler, K., and Bentur, A.), Haifa, pp.279-290, 2001

[17] Bentur, A., Igarashi, S., and Kovler, K.: Control of autogenous shrinkage and cracking of high strength concrete, Proc. 5th International Symposium on High Strength /High Performance Concrete, Sandefjord, Norway, Vol.2, pp.1017-1026, 1999
[18] Kohno, K., Okamoto, T., Ishikawa, Y., et al: Effects of artificial lightweight aggregate on autogenous shrinkage of concrete, Cement and Concrete Research, Vol.29, No.4, pp.611-614, 1999
[19] Zhang, M.-H., and Gjorv, O.E.: Effect of silica fume on pore structure and chloride diffusivity of low porosity cement pastes, Cement and Concrete Research, Vol.21, No.6, pp.1006-1014, 1991
[20] Park, K.B., Noguchi, T., and Tomosawa, F.: A study on the hydration ratio and autogenous shrinkage of cement paste, Autogenous Shrinkage of Concrete, Proc. Intl. Workshop on Autogenous Shrinkage of Concrete, AUTOSHRINK'98 (ed. Tazawa, E.), JCI, Tokyo, pp.281-290, 1998
[21] Wu, Z.-Q., and Young, J.F.: The hydration of tricalcium silicate in the presence of colloidal silica, J. Materials Science, Vol.19, No.11, pp.3477-3486, 1984
[22] Paillere, A.M., Buil, M., and Serrano, J.J.: Effect of fiber addition on the autogenous shrinkage of silica fume concrete, ACI Materials Journal, Vol.86, No.2, pp.139-144, 1989
[23] Dela, B.F., and Stang, H.: Crack formation around aggregate in high shrinkage cement paste, Fracture Mechanics of Concrete Structures, Proc. of FRAMCOS-3 (eds. Mihashi, H., and Rokugo, K.), AEDIFICATIO, Freiburg, Vol.1, pp.233-242, 1998
[24] Tazawa, E., and Miyazawa, S.: Influence of constituents and composition on autogenous shrinkage of cementitious materials, Magazine of Concrete Research, Vol.49, No.178, pp.15-22, 1997
[25] Iriya, K., Hattori, T., and Umehara, H.: Study on characterization of compressive and tensile creep behavior for early aged concrete, Journal of Materials, Concrete Structures and Pavements, No.599/V-40, pp.105-117, 1998
[26] Hadley, D.W.: The nature of paste-aggregate interface, Ph.D. Thesis, Purdue University, 1972
[27] Kjellsen, K.O., and Atlassi, E.H.: Pore structure of silica fume systems, Presence of hollow-shell pores, Cement and Concrete Research, Vo.29, No.1, pp.133-142, 1999
[28] van Breugel, K., and Lokhorst, S.J.: The role of microstructural development on creep and relaxation of hardening concrete, Proc. of RILEM Intl. Conf. on Early Age Cracking in Cement Systems (eds. Kovler, K., and Bentur, A.), Haifa, pp.3-10, 2001